

# PROTON COMPUTED TOMOGRAPHY BASED ON RICHARDSON–LUCY ALGORITHM

ÁKOS SUDÁR<sup>1,2</sup> AND GERGELY GÁBOR BARNAFÖLDI<sup>1</sup>  
FOR THE BERGEN PCT COLLABORATION

**ABSTRACT.** Objective: Proton therapy is a emerging method against cancer. One of the main development is to increase the accuracy of the Bragg-peak position calculation, which requires more precise relative stopping power (RSP) measurements. An excellent choice is the application of proton computed tomography (pCT) systems which take the images under similar conditions to treatment as they use the same irradiation device and hadron beam for imaging and treatment. A key aim is to develop an accurate image reconstruction algorithm for pCT systems to reach their maximal performance.

**Approach:** An image reconstruction algorithm was developed in this work, which is suitable to reconstruct pCT images from the energy, position and direction measurement of individual protons. The flexibility of an iterative image reconstruction algorithm was utilised to appropriately model the trajectory of protons. Monte Carlo (MC) simulations of a Derenzo and a CTP404 phantom was used to test the accuracy of the image reconstruction.

**Main results:** The Richardson–Lucy algorithm was applied first and successfully for pCT image reconstruction. Probability density based approach was applied for interaction (system) matrix generation, which is an advanced approach to consider the uncertain path of the protons in the patient.

**Significance:** The track of protons are scattered when they travel through material at the hadron therapy energies. This property limits the achievable spatial resolution, especially for single-sided pCT setups investigated in this study. The main motivation of the presented research is to test new approaches for the image reconstruction, focusing on the achieved spatial- and density resolution and the image noise. Realistic imaging setup were simulated with reasonably low proton statistics, to achieve results, which is likely to be reproducible in clinical environment.

## 1. INTRODUCTION

Hadron therapy is an emerging and efficient curing method against cancer. The increasing number of hadron therapy centers and the number of successful treatments presents its success. Today’s accelerator techniques led us to use protons or heavier ions as bombarding particles. The application of hadron beams instead of X-ray results more focused dose distribution (M. Durante, Orecchia, and J. Loeffler, 2017). Indeed, using higher mass number beams than proton (He, C and O) can results an increased relative biological effectiveness (RBE) in the tumor volume, while keep the RBE close to one in healthy tissues (Marco Durante, Debus, and J. S. Loeffler, 2021). The higher the dose gradient around the treated volume requires the lower uncertainty in the relative stopping power (RSP) distribution during dose planning, to avoid insufficient dosage of the tumor or the overdose of organs at risk.

The development of proton Computed Tomography (pCT) techniques are promising solutions for the above problems. Applying the same irradiation device, beam, and hadron for both the medical imaging and the treatments can significantly reduce the uncertainties of the imaging. To obtain this, two main imaging strategies are exist:

- (i) The first concept is to measure the average energy loss of the proton beam. This design is feasible from a technical point of view, but can only achieve poor spatial resolution with the clinically available proton beams (Krah et al., 2018).
- (ii) The second concept is the so called *list mode* imaging concept, which measures the energy loss and in parallel it estimates the path of each individual proton. Monte Carlo (MC) simulations and prototype measurements showed that this solution can meet the required spatial and density resolutions, so the focus is moved toward this direction (Robert P Johnson, 2017).

Nowadays, the pCT scanner R&Ds around the world are tending to reach the prototyping and clinical/pre-clinical testing phase, which requires the integration of the prototype scanners into clinical environment. Following the list mode strategy, the path estimation of individual protons is usually based on the measurements of the upstream and downstream tracker detector pairs, which concept is called the *double-sided scanner design* (figure 1). One important further step can be the abandonment of the upstream tracker detectors and the application of a *single-sided scanner design*. The drawback of this latter concept is the less accurate proton path measurement, however the study by Sölle et al., 2020 concluded that the achievable spatial resolution meets the minimum requirement. Nevertheless with lower-precision proton path measurement compromises the spatial resolution of the scanner which immediately motivates the development and application of more accurate image reconstruction algorithms.

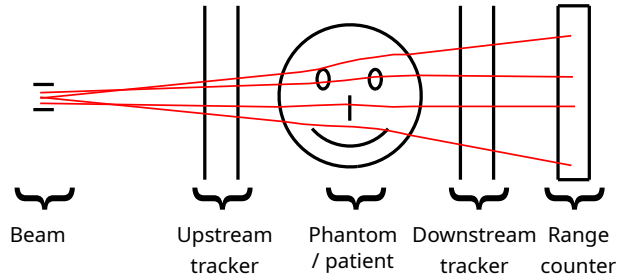


FIGURE 1. Detector design of the list mode imaging concept.

The realistic clinical applicability requires to complete the data taking in minutes, which result in 1-10 million protons per second measurement rate. The ultimate goal would be to finish the image capturing within the minimum gantry rotation time. The LLU/UCSC Phase-II Scanner prototype detector showed speed up to 1.2 million proton per second, which probably can be upgraded with 50% in the near future (Robert P. Johnson et al., 2016). To increase the data taking rate to 10 million protons per second, two possible directions exist: the first is to apply faster readout frequency of 10 MHz at least, the second is to measure multiple proton tracks within one readout frame. The second solution fits mostly with the single-sided scanner design, because this solution avoids the pairing problem of the upstream and downstream measurements, which leads to track confusion in case of a double-sided scanner even with low number of protons in a frame.

Multiple proton measurements fits best for silicon pixel trackers and silicon pixel sensor based range counters as presented by the Bergen pCT Collaboration (H. Pettersen et al., 2017; H. E. S. Pettersen et al., 2019; Alme et al., 2020). However, multiple proton measurements can be done by applying three silicon strip detectors rotated relative to each other as presented by the PRAVDA collaboration (Esposito et al., 2018). Another layout has been designed by the iMPACT group. The ProXY detector combines the two acceleration possibilities with monolithic active pixel detectors. Applying this layout, about 50 MHz readout frequency can be reached, and it is planned to measure multiple-proton events (Mattiazzo et al., 2015).

In this paper authors present for the first time a novel points, which may be applied in the proposed pCT detector concepts: the Richardson–Lucy algorithm (Richardson, 1972; Lucy, 1974) was applied for the image reconstruction of a single-sided pCT scanner. The paper organized as follows: section 2 begins with the general approach to the image reconstruction problem itself, followed by the presentation of the details of the Richardson–Lucy algorithm and the proton-phantom interaction model. Section 3 compares detector designs and presents the applied Monte Carlo simulation. Section 3 also contains the evaluation of the spatial- and density resolution of phantoms. Results are summarized and discussed in section 4 and 5, respectively.

## 2. THE IMAGE RECONSTRUCTION ALGORITHM

The role of the image reconstruction is to give back the relative stopping power (RSP) distribution from the measured data. Two family of image reconstruction techniques exist: the first family contains the filtered backprojections, in contrast with the second includes the iterative reconstructions. The first family usually use integrals along straight lines, which seems to be an inaccurate approximation for the scattered proton trajectory. The so-called distance-driven backprojection belongs to this family but can take into account the curvature of the MLPs during the filtered backprojection (Rit et al., 2013). This method provides reasonably good spatial resolution however, it requires very high statistics, which might be not accepted by requirements of the clinical use. The second family of the image reconstructions models the imaging as the interaction of proton tracks and volumetric pixels (voxels) of the reconstruction space. This approach is suitable to handle curved proton trajectories and reaches reasonably good spatial and density resolution with acceptable statistics, however requires higher computational power. This method models the imaging as a large linear system of equations, which is described by the following general algebraic form:

$$\mathbf{y} = \mathbf{A} \cdot \mathbf{x}, \quad (1)$$

where  $\mathbf{y}$  is an  $m$ -dimensional vector, which has typically  $10^8$ - $10^9$  elements. The  $\mathbf{y}$  contains the water equivalent path length (WEPL) reduction of the protons in the reconstruction area. Variable  $\mathbf{x}$  is an  $n$ -dimensional vector (typically  $10^5$ - $10^7$  elements) containing the relative stopping power (RSP) of the voxels. Finally  $\mathbf{A}$  is the so called *system matrix*, which has  $n \times m$  elements of  $10^{13}$ - $10^{16}$ . The system matrix contains the interaction coefficients between protons and voxels. The information in matrix  $\mathbf{A}$  can be described as the (expected) length of the proton's path in the voxel. In practice,  $m$  is usually larger than  $n$ , so the linear equation system is over-determined. The

goal of the image reconstruction in general, is to determine the values of vector,  $\mathbf{x}$  with the knowledge of vector,  $\mathbf{y}$  and system matrix,  $\mathbf{A}$ .

Orthogonal projection based iterative algorithms are widely used for pCT image reconstruction as presented by Robert P Johnson, 2017; Gordon, Bender, and Gabor T. Herman, 1970; Penfold et al., 2010; Censor et al., 2008; G. T. Herman, 2009. In this work the authors applied the Richardson–Lucy deconvolution, which reached reasonable quality increase in the field of emission tomography (Shepp and Vardi, 1982), and have not been used earlier for proton computed tomography.

**2.1. The Richardson–Lucy Algorithm.** The Richardson–Lucy deconvolution iteration cycle (Richardson, 1972; Lucy, 1974) originating from the field of optics, and known as a fixed point iteration. The iterative solution is based on the formula,

$$\mathbf{x}_i^{k+1} = \mathbf{x}_i^k \frac{1}{\sum_j \mathbf{A}_{ij}} \sum_j \frac{\mathbf{y}_j}{\sum_l \mathbf{A}_{lj} \mathbf{x}_l^k} \mathbf{A}_{ij} , \quad (2)$$

for every  $i = 1, \dots, N$ , where  $N$  is the length of vector  $\mathbf{x}$ , which contains the RSP of the voxels,  $k$  is the number of iterations, matrix  $\mathbf{A}_{ij}$  contains the interaction coefficients between the proton trajectories and the voxels,  $j = 1, \dots, M$  is the index of the trajectories, where  $M$  is the number of the trajectories,  $\mathbf{y}_j$  contains the integrated RSP along the trajectories, which is equivalent with the WEPL reduction of the protons travelling along the trajectories. The  $\mathbf{y}_j / \sum_l \mathbf{A}_{lj} \mathbf{x}_l^k$  term is usually called Hadamard ratio, and it represents the ratio of the integrated RSP along the proton path and its estimate based on the voxel values calculated in the previous iteration.

**2.2. The Proton-Phantom Interaction.** Instead of the most simple straight line approximation, the literature uses the estimated (most likely) path of the protons, based on the upstream and downstream measurements of proton track position and angle in case of a double-sided scanner design. Novel formulae are available in (Schneider, 1994; Williams, 2004; Schulte et al., 2008; Krah et al., 2018) to calculate the most likely path (MLP) of the protons. In case of a single-sided scanner design, where upstream measurements are not available, the beam information is used. Certainly, this contains much more uncertainty than a precise measurement. In this work the authors followed the formalism of Krah et al., 2018 as it considers the uncertainty of the measurements and the beam. The path of the protons was considered to be straight outside the phantom.

In this article the authors applied an advanced approach suggested by Williams, 2004: a Gaussian probability density distribution of the real proton path around the MLP, which takes into account the uncertain path of the protons in the phantom. This approach was used by Wang, Mackie, and Tomé, 2010 for pCT image reconstruction. An average standard deviation was considered during the proton path in the patient, which is an approximation compared to the depth dependent probability density investigated by Williams, 2004, which work did not deal with image reconstruction. The average standard deviation was chosen based on the experience of the authors during the development.

### 3. SIMULATIONS WITH THE ALGORITHM

The ultimate goal of pCT imaging for proton therapy is to provide a stable basis for accurate dose planning. However, it is a challenge to define a measure, which characterizes the goodness of a reconstructed RSP distribution for dose calculation. Instead of this missing ideal measurement, general image properties (spatial and density resolution, image noise) are usually used to quantify image quality. To study this, the imaging of dedicated spatial and density resolution phantoms was simulated with Monte Carlo techniques, reconstructed by the formerly described method and evaluated following the instructions later on this section.

**3.1. The Proton CT Scanner Model.** A single-sided detector design (figure 2) with a 230 MeV/u pencil beam was investigated. The full width at half maximum (FWHM) of the Gaussian beam was 7 mm (with about 3 mm standard deviation), the spot divergence was set to 2.8 mrad and the spot emittance was 3.0 mrad×mm, following the beam model of Sølvi et al., 2020. Three different detector layer was investigated: the first is an idealized detector with no measurement errors, the second is a silicon pixel tracker modelled after the design of the Bergen pCT Collaboration (H. E. S. Pettersen et al., 2019; Alme et al., 2020) and the third is a silicon strip detector based tracker layer followed the LLU/UCSC Phase-II Scanner design of the Loma Linda University (LLU) and the University of California at Santa Cruz (UCSC) (Robert P. Johnson et al., 2016). We note, that the results of this work is valid for an envisioned single-sided scanner, built of the LLU/UCSC Phase-II Scanner tracker layers, in comparison with the existing LLU/UCSC Phase-II Scanner which is a state-of-the-art double-sided setup.

The properties of the three detector layer setups, the idealized, the silicon pixel, and the silicon strip, are summarized in table 1. The idealized setup is a single sensitive layer, but in the latter two realistic cases each tracker layer contains two sensitive planes due to the existing technological solutions (figure 2). If the detection is

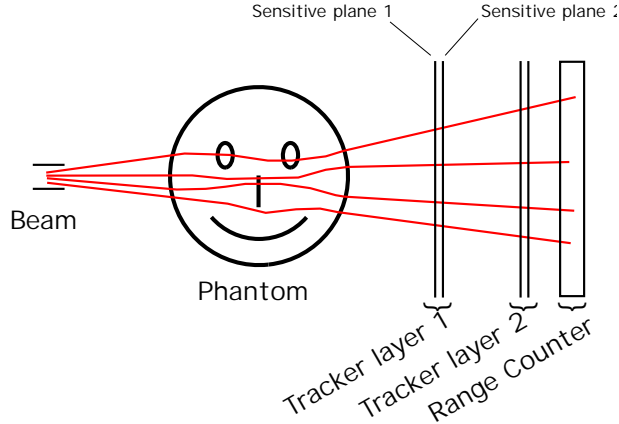


FIGURE 2. Single-sided list mode detector design.

based on a silicon pixel detector a double structure of two equivalent sensitive planes need to apply to fully cover the alternating sensitive and readout electronics panels. While applying silicon strip detectors, two separate planes are required for the perpendicular  $x$  and  $y$  directions. Table 1 contains the joint material budget of these double layers. The WEPL resolution of both realistic setups was chosen to be 3 mm (standard deviation of a normal distribution), which was added to the simulated range straggling in the phantom. This is a realistic uncertainty, however this is a very rudimentary model, as the measurement error is likely to depend on the remaining range of the protons behind the patient. The distance of the first detector pair to the rotation axis (isocenter) was chosen for 400 mm in all cases, which result in 300 mm and 325 mm detector-phantom distance for the Derenzo and the CTP404 phantoms, respectively. Similar distances are used for portal detectors applied in photon therapy gantries, so they can be considered to be realistic for the future pCT devices as well (Krah et al., 2018).

	Unit	Ideal setup	Silicon pixel	Silicon strip
Layer material budget ( $x/X_0$ )	-	0	$4.2 \times 10^{-3}$	$8.5 \times 10^{-3}$
Distance between layers	mm	-	50	50
Spatial resolution	$\mu\text{m}$	0	5	66
Angular resolution (130-230 MeV/u)	mrad	0	1.7-2.9	3.1-4.6
Correlation (130-230 MeV/u)	mrad $\times$ mm	0	$-5 \times 10^{-4}$	$-8.7 \times 10^{-2}$
Statistical WEPL resolution	mm	0	3.0	3.0

TABLE 1. Comparison of tracker detector pair model parameters: Ideal setup, with no measurements errors, Silicon pixel detector based on the design of the Bergen pCT Collaboration (H. E. S. Pettersen et al., 2019; Alme et al., 2020), and Silicon strip detector model following the structure of the LLU/UCSC Phase-II Scanner (Robert P. Johnson et al., 2016).

**3.2. The Applied Phantoms.** To test and validate the application of Richardson–Lucy algorithm was required to apply standardised evaluation methods. Therefore, we applied two widely-applied phantom in our analysis. In this study the RSP distribution was reconstructed in one plane of the phantoms, so the phantoms were considered to be offset invariant in the direction of the rotation axis. To ensure the offset invariance 400 mm high phantoms were simulated in the axis direction.

The spatial resolution of the reconstruction was measured with the MC imaging of the Derenzo phantom: a 200 mm diameter water cylinder, which contains six sectors of 1.5-6 mm diameters aluminium rods, specially chosen for the current analysis. The original idea of this phantom comes by Derenzo et al., 1977.

We also used a CTP404 phantom for our study. CTP404 is produced by The Phantom Laboratory, 2022, and designed to measure how accurately a material property is reconstructed in a homogeneous region of the phantom. The reconstruction accuracy of the RSP can be evaluated for proton CT imaging, also referred to as density resolution in the literature. The CTP404 phantom is an epoxy 150 mm diameter cylinder, which contains 8 different material inserts with a diameter of 12.2 mm. The average RSP of the inserts was evaluated in an 8 mm diameter circle in the middle of the inserts and compared to the real RSP values investigated by Alme et al., 2020. The standard deviation of the RSP was also evaluated in every inserts to characterise the noise of the image.

**3.3. Steps of the Simulation with the Algorithm.** A simulation code was developed to test the Richardson–Lucy algorithm, which was divided into the following steps (schematic in figure 3.3):

- (1) The data taking was simulated with Monte Carlo method. The beam and the phantom were modeled appropriately in the simulation. The Geant4 (version 11.0.0) (Agostinelli et al., 2003; Allison et al., 2006) was used with GATE (version 9.2) (Jan, Santin, et al., 2004; Jan, Benoit, et al., 2011). In the reference physics list settings QGSP\_BIC\_EMY was activated for the calculations. Data taking of one slice was simulated from 180 directions in  $2^\circ$  steps. Field of view (FOV) with 220 mm was applied for the Derenzo phantom (111 beam positions with 2 mm steps), and 170 mm FOV was used in case of the CTP404 phantom (86 beam positions with 2 mm steps). Overall  $\sim 2$  million and  $\sim 1.5$  million primary protons were simulated from which  $\sim 1.2$  million and  $\sim 0.95$  million remains after 3 sigma filtering in case of the Derenzo and the CTP404 phantoms, respectively. Instead of modeling the detector in the MC simulation, the exact position, direction and energy of the protons were read out at the position of the first tracker layer, and the measurement uncertainties were assigned in the next step.
- (2) In this step the errors of position and direction measurements were drawn from correlated Gaussian distributions and added to the exact positions and directions of simulated protons. The measurement uncertainty was calculated based on the guideline of Krah et al., 2018. The WEPL measurement error also was randomly assigned from a Gaussian distribution to the WEPL of the protons calculated from their energy losses, simulated in the previous step. The parameters from table 1 were used. In case of the ideal setup this step was certainly skipped, since the lack of errors/uncertainties of the idealized case.
- (3) A 3 sigma filtering is applied for the direction and WEPL of the protons originating from the same beam spot. The goal of this step was to filter out protons, which undergo nuclear collisions in the patient. This type of filtering was suggested and used by Schulte et al., 2008.
- (4) Calculation of the most probable incoming and outgoing position of the protons on a cylinder around the phantom is performed. In this step the formalism of Krah et al., 2018 was applied. The diameter of the cylinder was chosen to be 10 mm wider than that of the phantom in order to avoid artefacts.
- (5) The Richardson–Lucy algorithm was used to reconstruct the RSP distribution from the individual proton histories. On the fly system matrix calculation was applied based on simplified probability density around a third order spline approximation of the MLP.
- (6) In the final step the spatial resolution was evaluated based on the reconstruction of the Derenzo phantom. The density resolution and the image noise were calculated from the reconstructed CTP404 phantom.

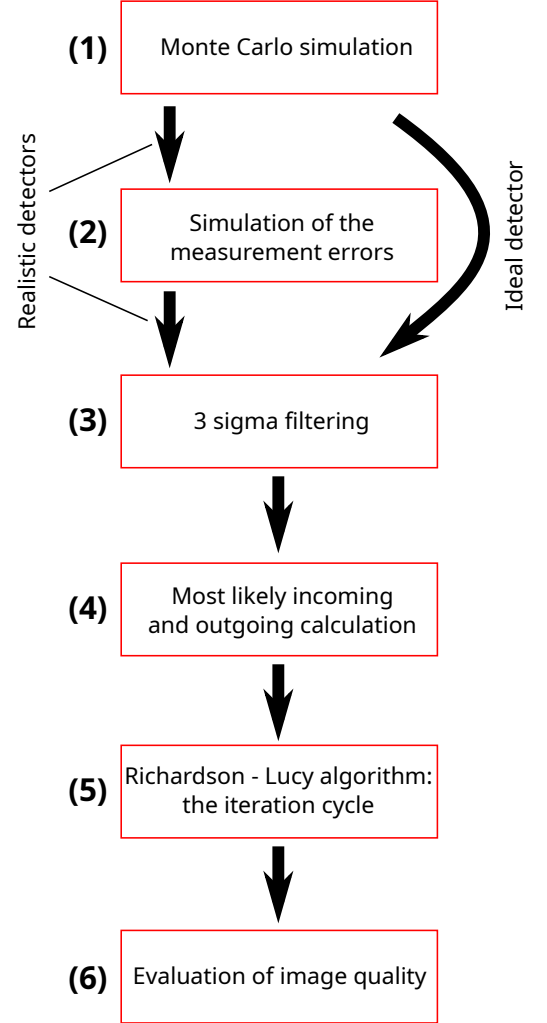


FIGURE 3. Simulation steps.

Calculations were done on the machines of the Wigner Scientific Computing Laboratory’s hardware. The computationally demanding part of the algorithm was running on four 1080 Ti GPU cards. The focus of the current

work was on the proof of the concept of probability density based system matrix calculation with Richardson–Lucy reconstruction algorithm, so the authors did not focus on the optimization of the implemented code.

**3.4. Evaluation of the Derenzo Phantom.** The evaluation of the measured phantom is based on the above simulation, and starts with the comparison of the reconstructed intensity in the position of the aluminium rods (peaks) and medium between them (valleys) as it is demonstrated in figure 4. After subtraction of the background (defined by the tails of the distribution) the valley-to-peak ratio can be calculated.

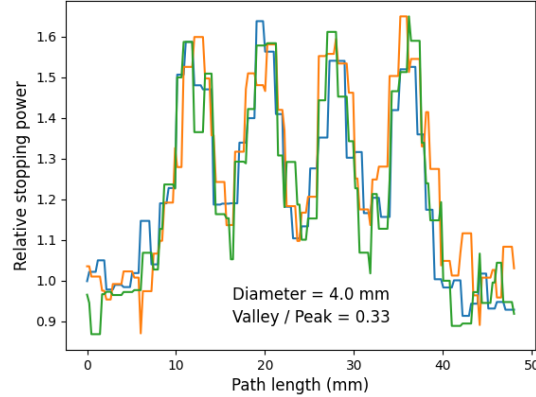


FIGURE 4. The RSP distribution along the sidelines (with three different colors) of the triangle from the 4 mm rods in the reconstructed Derenzo phantom. The Bergen pCT setup was applied.

The blurring effect of the reconstruction is modeled as a convolution with the so called point-spread function. It is a Gaussian function, and its Fourier transform is the modulation transfer function (MTF). The frequency of the MTF at 10 % (measured in units of line pair per cm) can be derived from the valley-to-peak ratio (figure 5) and quantifies the spatial resolution of the reconstructed image. If the valley-to-peak ratio is too close to zero or one the image noise suppress the information about the point-spread function, so a sector of the Derenzo phantom is suitable to cover only a limited resolution range. The phantom contains six sectors with different rod diameters to increase the range of resolution that can be evaluated.

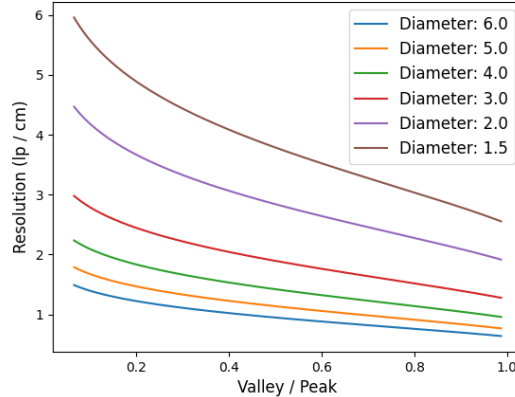


FIGURE 5. The spatial resolution (in the units of linepair per cm) as a function of the valley to peak ratio.

#### 4. RESULTS

As we pointed out earlier, in our study we investigated the simplified model with a single-sided detector setup. The center line of all beams falls into one perpendicular plane to the rotation axis. This image slice was reconstructed containing  $256 \times 256$  pixels with  $1 \text{ mm}^2$  size. Every proton was assigned to this layer, without taking into account the deviation of their path in the direction of the rotation axis. In the reconstruction step, every reconstructed image

was evaluated after 600 iterations as an optimum between the magnitude of spatial resolution and the image noise. The standard deviation ( $\sigma$ ) around the MLP of the protons were set about 0.4 mm, 0.5 mm and 1.0 mm according to the spatial uncertainty of the proton path for the ideal, silicon pixel and silicon strip detector layers, respectively.

The result of the reconstructed images of the Derenzo and CTP404 phantoms are shown in figure 6, on the left and right columns, respectively. Top row of the figure 6 presents the idealized case, which certainly the most

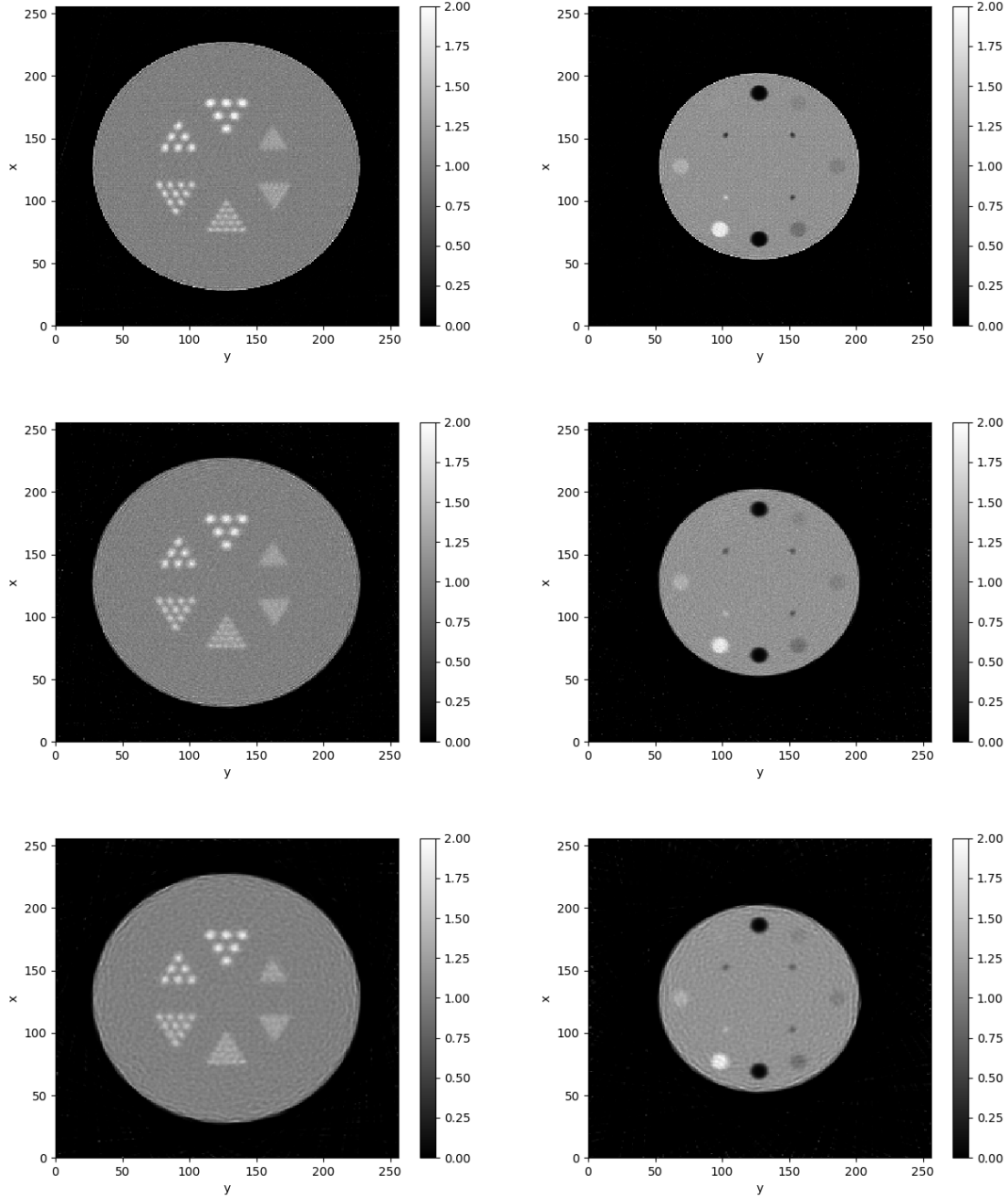


FIGURE 6. Richardson–Lucy algorithm based reconstruction of the Derenzo and CTP404 phantoms is presented on the left and right columns, respectively. From top to bottom the ideal, the pixel detector and the strip detector layers were drawn.

clearest reconstruction for both Derenzo and CTP404 phantoms. The middle and bottom rows are present more realistic imaging models with silicon pixel and silicon strip detectors, respectively. It is clearly visible that as the position and direction measurement uncertainties increases, the spatial resolution becomes worse and worse.

To quantify the quality of the above reconstructed images, the iteration-by-iteration evolution of the spatial resolution, the image noise and the density resolution are drawn in figure 7, respectively, from left to right. The spatial resolution (left panel) of the ideal setup was found to be 2.4 lp/cm for the ideal setup, 2.0 lp/cm and 1.5 lp/cm for the silicon pixel and the silicon strip detector based setups, respectively. The noise (middle panel) of the ideal and silicon pixel setups seems to be similar (5 % and 4.8 %, respectively), while the silicon strip detector based setup reached significantly lower noise (3.3 %). This observation indicates that if the number of protons are fixed, then the  $\sigma$  of the reconstruction has the most important effect on noise, instead of spatial or WEPL measurement uncertainties. We note, that the value of  $\sigma$  parameter was set significantly higher in case of the silicon strip setup, following the higher uncertainty in the proton path measurement compared with the other two detector layers.

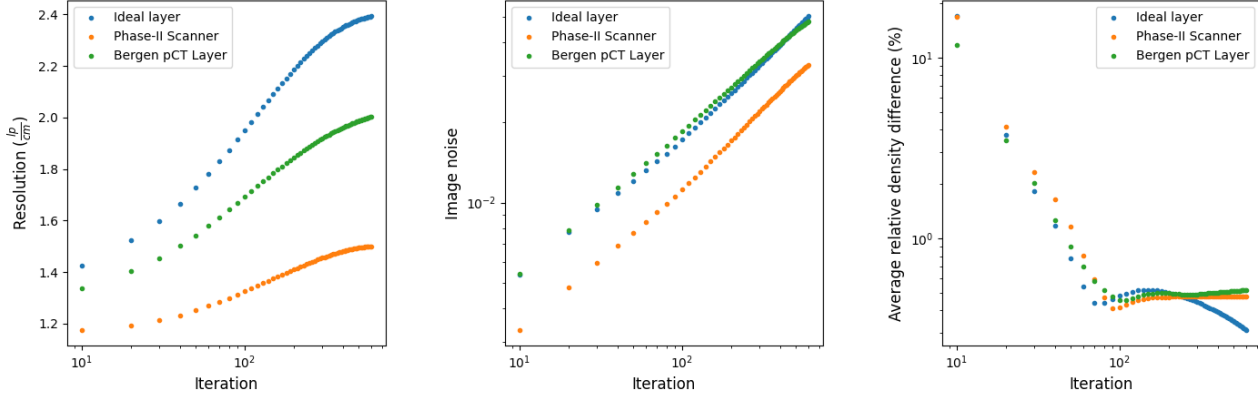


FIGURE 7. Left: the spatial resolution, middle: the image noise and right: the average relative RSP error as a function of the iteration number.

The error of the density reconstruction is quickly decreasing up to 70-90 iterations, thereafter all saturates, while for the ideal setup it is getting better at large iteration numbers. The average relative RSP difference (except air) was found to be 0.3 % for the ideal and 0.5 % for the realistic setups after 600 iterations. The RSP of the air instead of the real 0.001 was found to be 0.036, 0.051 and 0.061 for the ideal, the silicon pixel and the silicon strip setups. The density resolution of the tissues around and above water can be obviously reconstructed with better accuracy than the required 1 % (Poludniowski, Allinson, and Evans, 2015), but the density resolution is pure for low density regions. The reconstructed RSP of the air inserts was significantly decreasing even after 600 iterations, so even more iterations may solve this uncertainty. The RSP of all inserts (instead of air) was underestimated, most likely caused by the overestimated RSP of the air around the phantom. If the reconstruction area would be limited to the area of the phantom (instead of the whole  $256 \times 256 \text{ mm}^2$ ), the RSP estimation of these inserts probably would be even more accurate.

## 5. DISCUSSION

Based on our simulation, we found that the Richardson–Lucy algorithm with probability density based proton-phantom interaction reached 2.4 lp/cm spatial resolution for the ideal and 2.0 lp/cm resolution for a realistic setup. The density resolution was found to be significantly better than the required 1 % RSP accuracy, except of the low density region. We observed, that, the number of iterations further improves the spatial resolutions and in parallel the density resolution at low RSP as well. Meanwhile, the larger noise (around 5 % after 600 iterations) limits the applicable number of iterations. This limitation could be exceeded by imaging with higher statistics or maybe by implementing superiorization, which reduces the noise.

## 6. SUMMARY

In this work the application of the Richardson–Lucy algorithm with probability density based proton-phantom interaction calculation for proton CT image reconstruction has been presented. The authors applied clinically realistic setups and parameters in the Monte Carlo simulations: 400 mm detector-isocenter distance, 1.5-2 million primary protons per image slice and realistic beam and detector characteristics. For testing and for the evaluation of the resolutions two widely used phantom were applied the Derenzo and the CTP404.



The authors concluded that the presented reconstruction method meets the required density resolution, and have similar density resolution as the state of art prototypes. However, the spatial resolution of the images are promising, but has not reached the clinical requirements yet. Further development of the algorithm is necessary. It is also important to mention, that however the reconstructed images are noisy due to the low statistics, they are almost artefact free without the application of any post processing method.

The authors are continuing the algorithm development, with a focus on the spatial resolution and reconstruction time, which limited the investigations of the current work to only one layer. Indeed the possibility of the speedup of the algorithm has been also planned.

#### MEMBERS OF THE BERGEN PCT COLLABORATION

Max Ahle<sup>a</sup>, Johan Alme<sup>b</sup>, Gergely Gábor Barnaföldi<sup>c</sup>, Tea Bodova<sup>b</sup>, Vyacheslav Borshchov<sup>d</sup>, Anthony van den Brink<sup>e</sup>, Mamdouh Chaar<sup>b</sup>, Viljar Eikeland<sup>e</sup>, Gregory Feofilov<sup>f</sup>, Christoph Garth<sup>g</sup>, Nicolas R. Gauger<sup>a</sup>, Georgi Genov<sup>b</sup>, Ola Grøttvik<sup>b</sup>, Havard Helstrup<sup>h</sup>, Sergey Igolkin<sup>f</sup>, Ralf Keidel<sup>i</sup>, Chinorat Kobdaj<sup>j</sup>, Tobias Kortus<sup>i</sup>, Viktor Leonhardt<sup>g</sup>, Shruti Mehendale<sup>b</sup>, Raju Ningappa Mulawade<sup>i</sup>, Odd Harald Odland<sup>k, b</sup>, George O'Neill<sup>b</sup>, Gábor Papp<sup>l</sup>, Thomas Peitzmann<sup>e</sup>, Helge Egil Seime Pettersen<sup>k</sup>, Pierluigi Piersimoni<sup>b, m</sup>, Maksym Protsenko<sup>d</sup>, Max Rauch<sup>b</sup>, Attiq Ur Rehman<sup>b</sup>, Matthias Richter<sup>n</sup>, Dieter Röhrich<sup>b</sup>, Joshua Santana<sup>i</sup>, Alexander Schilling<sup>i</sup>, Joao Seco<sup>o, p</sup>, Arnon Songmoolnak<sup>b, j</sup>, Jarle Rambo Sølvi<sup>q</sup>, Ákos Sudár<sup>c, r</sup>, Ganesh Tambave<sup>b</sup>, Ihor Tymchuk<sup>d</sup>, Kjetil Ullaland<sup>b</sup>, Monika Varga-Kofarago<sup>c</sup>, Lennart Volz<sup>s, t</sup>, Boris Wagner<sup>b</sup>, Steffen Wendzel<sup>i</sup>, Alexander Wiebel<sup>i</sup>, RenZheng Xiao<sup>b, u</sup>, Shiming Yang<sup>b</sup>, Hiroki Yokoyama<sup>e</sup>, Sebastian Zillien<sup>i</sup>

a) Chair for Scientific Computing, TU Kaiserslautern, 67663 Kaiserslautern, Germany; b) Department of Physics and Technology, University of Bergen, 5007 Bergen, Norway; c) Wigner Research Centre for Physics, Budapest, Hungary; d) Research and Production Enterprise “LTU” (RPELTU), Kharkiv, Ukraine; e) Institute for Subatomic Physics, Utrecht University/Nikhef, Utrecht, Netherlands; f) St. Petersburg University, St. Petersburg, Russia; g) Scientific Visualization Lab, TU Kaiserslautern, 67663 Kaiserslautern, Germany; h) Department of Computer Science, Electrical Engineering and Mathematical Sciences, Western Norway University of Applied Sciences, 5020 Bergen, Norway; i) Center for Technology and Transfer (ZTT), University of Applied Sciences Worms, Worms, Germany; j) Institute of Science, Suranaree University of Technology, Nakhon Ratchasima, Thailand; k) Department of Oncology and Medical Physics, Haukeland University Hospital, 5021 Bergen, Norway; l) Institute for Physics, Eötvös Lóránd University, 1/A Pázmány P. Sétány, H-1117 Budapest, Hungary; m) UniCamillus – Saint Camillus International University of Health Sciences, Rome, Italy; n) Department of Physics, University of Oslo, 0371 Oslo, Norway; o) Department of Biomedical Physics in Radiation Oncology, DKFZ—German Cancer Research Center, Heidelberg, Germany; p) Department of Physics and Astronomy, Heidelberg University, Heidelberg, Germany; q) Department of Diagnostic Physics, Division of Radiology and Nuclear Medicine, Oslo University Hospital, Oslo, Norway; r) Budapest University of Technology and Economics, Budapest, Hungary; s) Biophysics, GSI Helmholtz Center for Heavy Ion Research GmbH, Darmstadt, Germany; t) Department of Medical Physics and Biomedical Engineering, University College London, London, UK; u) College of Mechanical & Power Engineering, China Three Gorges University, Yichang, People’s Republic of China

#### ACKNOWLEDGEMENT

The authors would like to thank the support of the Hungarian National Research, Development and Innovation Office (NKFIH) grants under the contract numbers OTKA K135515 and 2019-2.1.6-NEMZ-KI-2019-00011, 2020-2.1.1-ED-2021-00179. This work was also supported by the Research Council of Norway (Norges forskningsrad) and the University of Bergen, grant number 250858. The authors acknowledge the support os Trond Mohn Foundation (BFS2017TMT07). Computational resources were provided by the Wigner Scientific Computing Laboratory (WSCLAB).

## REFERENCES

- Agostinelli, S., J. Allison, K. Amako, et al. (2003). “Geant4—a simulation toolkit”. In: *Nuclear Instruments and Methods in Physics Research Section A: Accelerators, Spectrometers, Detectors and Associated Equipment* 506.3, pp. 250–303. ISSN: 0168-9002. DOI: [https://doi.org/10.1016/S0168-9002\(03\)01368-8](https://doi.org/10.1016/S0168-9002(03)01368-8).
- Allison, J., K. Amako, J. Apostolakis, et al. (2006). “Geant4 developments and applications”. In: *IEEE Transactions on Nuclear Science* 53.1, pp. 270–278. DOI: 10.1109/TNS.2006.869826.
- Alme, Johan, Gergely Gábor Barnaföldi, Rene Barthel, et al. (2020). “A High-Granularity Digital Tracking Calorimeter Optimized for Proton CT”. In: *Frontiers in Physics* 8. ISSN: 2296-424X. DOI: 10.3389/fphy.2020.568243.
- Censor, Yair, Tommy Elfving, Gabor T. Herman, et al. (Jan. 2008). “On Diagonally Relaxed Orthogonal Projection Methods”. In: *SIAM Journal on Scientific Computing* 30 (1). DOI: 10.1137/050639399.
- Derenzo, S. E., T. F. Budinger, J. L. Cahoon, et al. (1977). “High Resolution Computed Tomography of Positron Emitters”. In: *IEEE Transactions on Nuclear Science* 24.1, pp. 544–558. DOI: 10.1109/TNS.1977.4328738.
- Durante, M., R. Orecchia, and JS. Loeffler (2017). “Charged-particle therapy in cancer: clinical uses and future perspectives”. In: *Nat Rev Clin Oncol* 14.8, pp. 483–495. DOI: 10.1038/nrclinonc.2017.30.
- Durante, Marco, Jürgen Debus, and Jay S. Loeffler (2021). “Physics and biomedical challenges of cancer therapy with accelerated heavy ions”. In: *Nature Reviews Physics* 3.12, pp. 777–790. ISSN: 2522-5820. DOI: 10.1038/s42254-021-00368-5.
- Esposito, Michela, Chris Waltham, Jonathan T. Taylor, et al. (2018). “PRaVDA: The first solid-state system for proton computed tomography”. In: *Physica Medica* 55, pp. 149–154. ISSN: 1120-1797. DOI: <https://doi.org/10.1016/j.ejmp.2018.10.020>.
- Gordon, Richard, Robert Bender, and Gabor T. Herman (1970). “Algebraic Reconstruction Techniques (ART) for three-dimensional electron microscopy and X-ray photography”. In: *Journal of Theoretical Biology* 29.3, pp. 471–481. ISSN: 0022-5193. DOI: [https://doi.org/10.1016/0022-5193\(70\)90109-8](https://doi.org/10.1016/0022-5193(70)90109-8).
- Herman, G. T. (2009). *Fundamentals of Computerized Tomography*. 2nd ed. Springer.
- Jan, S., D. Benoit, E. Becheva, et al. (Jan. 2011). “GATE V6: a major enhancement of the GATE simulation platform enabling modelling of CT and radiotherapy”. In: *Physics in Medicine and Biology* 2011-jan 20 vol. 56 iss. 4 56 (4). DOI: 10.1088/0031-9155/56/4/001.
- Jan, S., G. Santin, D. Strul, et al. (Sept. 2004). “GATE: a simulation toolkit for PET and SPECT”. In: *Physics in Medicine and Biology* 2004-sep 10 vol. 49 iss. 19 49 (19). DOI: 10.1088/0031-9155/49/19/007.
- Johnson, Robert P (Nov. 2017). “Review of medical radiography and tomography with proton beams”. In: *Reports on Progress in Physics* 81 (1). DOI: 10.1088/1361-6633/aa8b1d.
- Johnson, Robert P., Vladimir Bashkirov, Langley DeWitt, et al. (Feb. 2016). “A Fast Experimental Scanner for Proton CT: Technical Performance and First Experience With Phantom Scans”. In: *IEEE Transactions on Nuclear Science* 63 (1). DOI: 10.1109/TNS.2015.2491918.
- Krah, Nils, Feriel Khellaf, Jean Michel Letang, et al. (July 2018). “A comprehensive theoretical comparison of proton imaging set-ups in terms of spatial resolution”. In: *Physics in Medicine and Biology* 63 (13). DOI: 10.1088/1361-6560/aaca1f.
- Lucy, L. B. (June 1974). “An iterative technique for the rectification of observed distributions”. In: *Astronomical Journal* 79. Provided by the SAO/NASA Astrophysics Data System, p. 745. DOI: 10.1086/111605.
- Mattiazzo, S., D. Bisello, P. Giubilato, et al. (Apr. 2015). “Advanced proton imaging in computed tomography”. In: *Radiation Protection Dosimetry* 166 (1-4). DOI: 10.1093/rpd/ncv197.
- Penfold, S. N., R. W. Schulte, Y. Censor, et al. (Oct. 2010). “Total variation superiorization schemes in proton computed tomography image reconstruction”. In: *Medical Physics* 37 (11). DOI: 10.1118/1.3504603.
- Pettersen, H.E.S., J. Alme, A. Biegun, et al. (2017). “Proton tracking in a high-granularity Digital Tracking Calorimeter for proton CT purposes”. In: *Nuclear Instruments and Methods in Physics Research Section A: Accelerators, Spectrometers, Detectors and Associated Equipment* 860, pp. 51–61. ISSN: 0168-9002. DOI: <https://doi.org/10.1016/j.nima.2017.02.007>.
- Pettersen, Helge Egil Seime, Johan Alme, Gergely Gábor Barnaföldi, et al. (2019). “Design optimization of a pixel-based range telescope for proton computed tomography”. In: *Physica Medica* 63, pp. 87–97. ISSN: 1120-1797. DOI: <https://doi.org/10.1016/j.ejmp.2019.05.026>.
- Poludniowski, G, N M Allinson, and P M Evans (Sept. 2015). “Proton radiography and tomography with application to proton therapy”. In: *British Journal of Radiology* 88 (1053). DOI: 10.1259/bjr.20150134.
- Richardson, William Hadley (Jan. 1972). “Bayesian-Based Iterative Method of Image Restoration”. In: *Journal of the Optical Society of America* 62 (1). DOI: 10.1364/JOSA.62.000055.
- Rit, Simon, George Dedes, Nicolas Freud, et al. (Feb. 2013). “Filtered backprojection proton CT reconstruction along most likely paths”. In: *Medical Physics* 40 (3). DOI: 10.1118/1.4789589.

- Schneider, Uwe (Nov. 1994). “Multiple Coulomb scattering and spatial resolution in proton radiography”. In: *Medical Physics* 21 (11). DOI: 10.1118/1.597212.
- Schulte, R. W., S. N. Penfold, J. T. Tafas, et al. (Oct. 2008). “A maximum likelihood proton path formalism for application in proton computed tomography”. In: *Medical Physics* 35 (11). DOI: 10.1118/1.2986139.
- Shepp, L. A. and Y. Vardi (1982). “Maximum Likelihood Reconstruction for Emission Tomography”. In: *IEEE Transactions on Medical Imaging* 1.2, pp. 113–122. DOI: 10.1109/TMI.1982.4307558.
- Sølie, Jarle Rambo, Lennart Volz, Helge Egil Seime Pettersen, et al. (July 2020). “Image quality of list-mode proton imaging without front trackers”. In: *Physics in Medicine and Biology* 65.13, p. 135012. DOI: 10.1088/1361-6560/ab8ddb.
- The Phantom Laboratory (2022). *Catphan® 600 phantom (containing CTP404 as a section)*. Last accessed 5 October 2022. URL: <https://www.phantomlab.com/catphan-600>.
- Wang, Dongxu, T. Rockwell Mackie, and Wolfgang A. Tomé (Aug. 2010). “On the use of a proton path probability map for proton computed tomography reconstruction”. In: *Medical physics* 37 (8). DOI: 10.1118/1.3453767.
- Williams, D C (June 2004). “The most likely path of an energetic charged particle through a uniform medium”. In: *Physics in Medicine and Biology* 49 (13). DOI: 10.1088/0031-9155/49/13/010.

<sup>1</sup>WIGNER RESEARCH CENTRE FOR PHYSICS, INSTITUTE FOR PARTICLE AND NUCLEAR PHYSICS, BUDAPEST, HUNGARY <sup>2</sup>BUDAPEST UNIVERSITY OF TECHNOLOGY AND ECONOMICS, INSTITUTE OF NUCLEAR TECHNIQUES, BUDAPEST, HUNGARY